

A NICMOS imaging study of high- z quasar host galaxies

Marek J. Kukula,^{1*} James S. Dunlop,¹ Ross J. McLure,² Lance Miller,²
 Will J. Percival,¹ Stefi A. Baum³ and Christopher P. O’Dea,³

¹*Institute for Astronomy, University of Edinburgh, Royal Observatory, Edinburgh EH9 3HJ, U.K.*

²*Nuclear and Astrophysics Laboratory, University of Oxford, Keble Road, Oxford, OX1 3RH, U.K.*

³*Space Telescope Science Institute, 3700 San Martin Drive, Baltimore, MD 21218, U.S.A.*

ABSTRACT

We present the first results from a major Hubble Space Telescope programme designed to investigate the cosmological evolution of quasar host galaxies from $z \simeq 2$ to the present day. Here we describe J and H -band NICMOS imaging of two quasar samples at redshifts of 0.9 and 1.9 respectively. Each sample contains equal numbers of radio-loud and radio-quiet quasars, selected to lie within the same narrow range of optical absolute magnitude ($-24 \geq M_V \geq -25$). Filter and target selection were designed to ensure that at each redshift the images sample the same part of the object’s rest-frame spectrum, longwards of 4000\AA where starlight from the host galaxy is relatively prominent, but avoiding potential contamination by $[\text{OIII}]\lambda 5007$ and $\text{H}\alpha$ emission lines.

At $z \simeq 1$ we have been able to establish host-galaxy luminosities and scalelengths with sufficient accuracy to demonstrate that the hosts of both radio-loud and radio-quiet quasars lie on the same Kormendy relation described by 3CR radio galaxies at comparable redshift (McLure & Dunlop 2000). Taken at face value the gap between the host luminosities of radio-loud and radio-quiet objects appears to have widened from only $\simeq 0.4$ mag. at $z \simeq 0.2$ (Dunlop et al. 2001) to $\simeq 1$ mag. at $z \simeq 1$, a difference that cannot be due to emission-line contamination given the design of our study. However, within current uncertainties, simple passive stellar evolution is sufficient to link these galaxies with the elliptical hosts of low-redshift quasars of comparable nuclear output, implying that the hosts are virtually fully assembled by $z \sim 1$.

At $z \simeq 2$ the hosts have proved harder to characterise accurately, and for only two of the nine $z \simeq 2$ quasars observed has it proved possible to properly constrain the scalelength of the host galaxy. However, the data are of sufficient quality to yield host-galaxy luminosities accurate to within a factor $\simeq 2$. At this redshift the luminosity gap between radio-loud and radio-quiet quasars appears to have widened further to $\simeq 1.5$ mag. Thus while the hosts of radio-loud quasars remain consistent with a formation epoch of $z > 3$, allowing for passive evolution implies that the hosts of radio-quiet quasars are $\simeq 2 - 4$ times less massive at $z \simeq 2$ than at $z \simeq 0.2$.

If the relationship between black-hole and spheroid mass is unchanged out to redshift $z \simeq 2$, then our results rule out any model of quasar evolution which involves a substantial component of luminosity evolution (e.g. Kauffmann & Haehnelt 2000). Rather, this study indicates that at $z \simeq 2$ there is a substantial increase in the number density of active black holes, along with a moderate increase in the fueling efficiency of a typical observed quasar. The fact that this latter effect is not displayed by the radio-loud objects in our sample might be explained by a selection effect arising from the fact that powerful radio sources are only produced by the most massive black holes (Dunlop et al. 2001; McLure & Dunlop 2000b).

Key words: quasars: general – galaxies: active – galaxies: evolution

1 INTRODUCTION

Recent years have brought great advances in our understanding of the symbiotic relationship between active galac-

* M.Kukula@roe.ac.uk

tic nuclei (AGN) and the galaxies in which they occur. Some of the most impressive advances concern quasars - the most powerful known AGN - as improvements in ground-based observing techniques and the advent of the Hubble Space Telescope (HST) have allowed the diffuse ‘fuzz’ of the underlying host galaxy to be reliably separated from the wings of the bright non-stellar nuclear point spread function (PSF) for the first time.

The problems inherent in observing quasar host galaxies from the ground are too well-known to require detailed explanation but, considering the enormous difficulties involved in separating faint, diffuse galaxy light from the PSF of a bright quasar, it is perhaps surprising that so much progress has been made to date using ground-based techniques. Although such studies are effectively limited to $z \leq 0.3$, at these low redshifts a combination of ground-based and HST programmes is beginning to yield a coherent picture of the properties of quasar hosts in the local universe.

However, the local universe is not the most representative region in which to study the quasar population: arguably the epoch of greatest importance to quasar research occurred at redshifts of $z \sim 2$ to 3 , when quasars were 2–3 orders of magnitude more numerous than they are today. Although simulations show that it is very difficult to derive the properties of quasar hosts at such high z from the ground with any degree of confidence (Taylor et al. 1996), numerous attempts have been made with (not surprisingly) confusing results. In this paper we present the results of a study using the Near-Infrared Camera and Multi-Object Spectrometer (NICMOS) on HST to investigate how the luminosities, sizes and morphologies of the hosts of both radio-loud and radio-quiet quasars (RLQs & RQQs) have evolved from the ‘golden era’ of quasar activity to the present day.

1.1 The host galaxies of low-redshift quasars

At low redshifts, attention has been focused on determining the luminosities, scalelengths, morphologies and interaction histories of quasar host galaxies, and investigating the extent to which these properties are correlated to the optical and radio luminosity of the quasar (Véron-Cetty & Woltjer 1990; Dunlop et al. 1993; McLeod & Rieke 1994a,b; Bahcall, Kirhakos & Schneider 1995a,b,1996; Hutchings & Morris 1995; Disney et al. 1995; Taylor et al. 1996; Bahcall et al. 1997; Hooper, Impey & Foltz 1997; Boyce et al. 1998; Carballo et al. 1998; McLeod, Rieke & Storrie-Lombardi 1999; Schade, Boyle & Letawsky 2000; Hamilton, Casertano & Turnshek 2001; Márquez et al. 2001). For example, it has long been known that low-luminosity AGN display marked preferences in terms of host type, with (radio-quiet) Seyferts favouring spiral hosts whilst (radio-loud) Radio Galaxies are exclusively associated with massive ellipticals. However, recent studies have demonstrated that this distinction breaks down at the higher redshifts and nuclear luminosities typical of radio-loud and radio-quiet quasars, and that powerful nuclear activity is predominantly associated with bulge-dominated galaxies, regardless of radio luminosity.

In our own HST study of low redshift ($0.1 \leq z \leq 0.25$), low luminosity ($-23 \leq M - V \leq -26$) RLQs and RQQs (McLure et al. 1999; Dunlop et al. 2001) we found that for quasars brighter than $M_R \sim -24$ the hosts are invariably massive elliptical galaxies with $L \geq 2L^*$, with typical scale-

lengths of ~ 10 kpc, and display a Kormendy relation identical to that of brightest cluster galaxies. This result is consistent with measurements of the massive dark objects in the nuclei of nearby inactive galaxies, which predict that only the largest spheroidal systems will harbour black holes of the requisite mass to produce luminous quasars (Kormendy & Richstone 1995; Magorrian et al. 1998; van der Marel 1999), and also with the discovery by McLeod & Rieke (1995) of a lower limit to the mass of a quasar host which is correlated with the luminosity of the quasar. The implication of these studies is that massive elliptical galaxies are the parent population of the quasar phenomenon. However, in a ground-based K -band study of luminous ($-25 \geq M_V \geq -27$) RQQs Percival et al. (2001) found evidence that, on scales much larger than those probed in optical HST images, some of the hosts are dominated by a disc component. Clearly the issue of host morphology has yet to be entirely resolved, but the finding that a quasar host requires at the very least a massive spheroidal component seems secure.

Spectral energy distributions (SEDs) also provide important information on the nature of the host galaxies. McLure et al. (1999) and Dunlop et al. (2001) found that the $R - K$ colours of their quasar hosts were consistent with normal passively-evolving elliptical galaxies with ages of ~ 12 Gyr, implying that the stellar populations formed at high redshift ($z \sim 3$). Optical off-nuclear spectroscopy of the same objects (Hughes et al. 2000; Nolan et al. 2001) confirms that, longwards of the 4000\AA break in their rest-frame spectra, these hosts are dominated by light from an old, well-established population of stars. Similar results are obtained for radio galaxies (e.g. de Vries et al. 2000).

1.2 High-redshift quasar hosts

The fact that the host galaxies of low-redshift quasars have mature stellar populations and contain a massive bulge component implies that, like local inactive elliptical galaxies, they are arguably consistent with the products of successive merger events. This raises important questions about the potential redshift dependence of the properties of quasar hosts. The dramatic cosmological evolution exhibited by the quasar population itself, with a comoving number density which peaks at redshifts of 2-3 before undergoing a rapid decline to its present low value, has been known for many years (e.g. Boyle et al. 1988; Dunlop & Peacock 1990; Warren, Hewett & Osmer 1994) but the extent and form of any evolution affecting quasar hosts remain as largely unknown quantities. The issue has been given renewed urgency by continuing efforts to characterise the starformation history of the universe, for which the redshift range of $z = 2 - 3$ also appears to correspond to an important epoch (Madau et al. 1996; Hughes et al. 1998; Steidel et al. 1999).

It is therefore important to determine how the luminosities, scalelengths, and the degree of morphological disturbance seen in quasar host galaxies varies with cosmological epoch between the peak of quasar activity at $z \simeq 2$ and the present day, and whether the hosts of radio-loud and radio-quiet quasars differ in their luminosity or morphological evolution. However, the difficulties involved in such studies are far more formidable than at low z and this is reflected in the confusion which surrounds the interpretation of ground-based attempts to observe high-redshift quasar hosts.

Several groups have attempted such observations from the ground and have succeeded in detecting extensions around high-redshift quasars (Hintzen, Romanishin & Valdes 1991; Heckman et al. 1991; Lehnert et al. 1992; Aretxaga, Boyle & Terlevich 1995; Rönnback et al. 1996; Aretxaga, Terlevich & Boyle 1998). These studies suggest that the host galaxies of quasars at $z \simeq 2$ are ~ 2.5 to 3 mag brighter than those of low-redshift quasars, a result which is consistent with common scenarios for elliptical galaxy evolution. However, the usefulness of any such direct comparison is confused by the fact that these high-redshift quasars are typically 5 magnitudes more luminous than the low-redshift objects studied to date. In addition, the observational situation is somewhat complex since other workers have failed to detect extended emission around high-redshift RQQs (Lowenthal et al. 1995). Hutchings (1995) also concludes that the hosts of RQQs are considerably fainter than those of RLQs at high redshift, a result which could however simply indicate that much of the light detected around high-redshift RLQs is not due to stars, but rather to processes associated with the extreme radio activity, as is found for high- z radio galaxies (Tadhunter et al. 1992), and for low- z RLQs (Stockton & MacKenty 1987). This emphasises the importance of avoiding emission lines and sampling the rest-frame spectrum longwards of the 4000Å break.

The study described in this paper attempts to avoid the problems outlined above by observing test samples of quasars over a range of redshifts out to $z = 2$ but limited to a narrow range of optical absolute magnitude ($-24 \leq M_V \leq -25$). Careful choice of filters ensures that our images always sample the same emission-line-free region of the object's restframe spectrum, thus avoiding any regions of extended [OIII] λ 5007 and H α emission which may be associated with the active nucleus. Thus, at each redshift we are always observing objects of roughly the same intrinsic luminosity, and in the same region (approximately V -band) of their rest-frame spectrum.

The layout of this paper is as follows. In section 2 we provide details of how our quasar samples were selected, and how the HST NICMOS observations were designed and implemented. The process of data reduction is described in section 3, including the details of how we chose to tackle the particular problems associated with producing NICMOS images of sufficient quality for a study of this type. In section 4 we explain how host-galaxy parameters were extracted from the data via 2-D modelling, and summarize the basic results of the image analysis. Then in section 5 we explore the implications of combining these new results with the results of our Cycle 6 HST study of quasar hosts at much lower redshift ($z \simeq 0.2$; McLure et al. 1999; Dunlop et al. 2001), and discuss our findings in the context of existing theoretical predictions. Finally, our results are summarized in section 6. For ease of comparison with existing results/predictions we assume an Einstein-de Sitter cosmology with $H_0 = 50 \text{ km s}^{-1} \text{ Mpc}^{-1}$ throughout most of this paper. However, in the penultimate section we focus on the implications of our results within the currently-favoured flat cosmological model with $\Omega_m = 0.3$, $\Omega_\Lambda = 0.7$ and $H_0 = 65 \text{ km s}^{-1} \text{ Mpc}^{-1}$.

2 THE OBSERVATIONS

Previous observations of quasar hosts with HST have demonstrated the importance of careful sample construction, the matching of samples and the selection of filter bandwidths to avoid the inclusion of strong emission lines. In this section we describe the selection criteria used in the construction of our quasar samples as well as the considerations which shaped the final observing strategy. The three samples resulting from these considerations, at $z \sim 0.4$, 1 and 2, are shown in Figure 1. The observations of the $z \sim 0.4$ sample, which use WFPC2 rather than NICMOS, were incomplete at the time of writing and discussion of the images of these objects is deferred to a subsequent paper. Details of the two high-redshift ($z \sim 1, 2$) samples, including redshifts, positions and observing dates, are given in Table 1. It is these two samples which are the subject of the present paper.

2.1 Sample design and choice of filters

2.1.1 Luminosity constraints

We have confined our selection of high-redshift quasars to the absolute magnitude range $-24 > M_V > -25$. This luminosity band is comparable to that of a subset of our low-redshift ($0.1 \leq z \leq 0.25$) quasar sample observed with WFPC2 on HST (McLure et al. 1999; Dunlop et al. 2001), allowing us to use this latter sample as a low-redshift baseline against which to measure any redshift-dependent change in the properties of the hosts for a narrow range of quasar luminosities. Also, experience from low- z studies, as well as the results of simulations using artificial quasar/host combinations and our 2-D modelling algorithm, demonstrates that in order to reliably recover the luminosities and scale-lengths of their host galaxies it is currently desirable to limit the high-redshift samples to quasars of such moderate-to-low optical luminosities.

2.1.2 Filter/redshift combinations

Having defined the luminosity range of the sample, the next priority was to break the flux-density/redshift correlation which inevitably arises in samples derived from flux-limited surveys, by ensuring that we sample a comparable range of luminosities at several different redshifts. However, to obtain a clean view of the starlight from the host galaxies at all redshifts it is also necessary to ensure that, as in our previous WFPC2 study at $z \simeq 0.2$, the spectrum of the host galaxy is always observed at $\lambda_{rest} > 4000\text{Å}$ and yet is uncontaminated by either [OIII] or H α line emission. In the $z \simeq 0.2$ study this entailed using the F675W filter on WFPC2. For the current study two NICMOS filters were selected: F110M (roughly J -band), which samples the desired rest-frame wavelengths for redshifts $0.83 \leq z \leq 1.00$; and F165M (roughly H -band), for $1.67 \leq z \leq 2.01$. A third filter, F184W (roughly I -band) on WFPC2, was also chosen to bridge the gap between the NICMOS observations and the McLure et al. (1999) low-redshift study by observing a third group of objects at $0.32 \leq z \leq 0.43$. (HST possesses slightly wider filters in all three of these wavelength regimes, but using these would have led to contamination by [OIII]

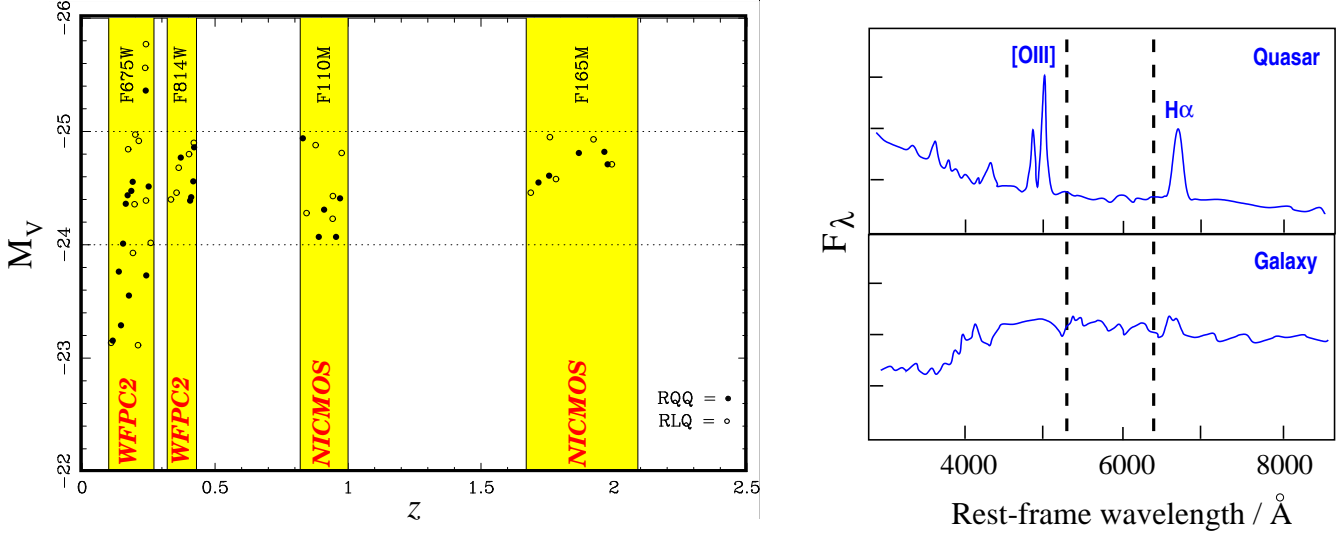


Figure 1. Left: Absolute V magnitude versus redshift for the RQQs (filled circles) and RLQs (open circles) in the current study. The shaded vertical bars represent the redshift regimes over which the indicated WFPC2 and NICMOS filters remain free from contamination by [OIII] λ 5007 and H α λ 6563 emission lines. Also shown are the quasars from our previous HST imaging study using WFPC2/F675W (McLure et al. 1999; Dunlop et al. 2001). This low- z sample spans almost 3 magnitudes in optical luminosity at a given redshift ($z \simeq 0.2$) whereas the three samples selected for the current study are confined to only 1 mag in luminosity but span the bulk of the history of the Universe. Thus these complementary low- z objects provide the baseline against which to measure any cosmological evolution in the high- z samples. Right: Schematic showing typical rest-frame spectra of a quasar (upper panel) and an early-type galaxy (lower panel). The two vertical lines delineate the region of the host-galaxy spectrum which is targeted by the redshift/filter combinations used in the observations described in this paper. Note the avoidance of prominent quasar emission lines and the increase in galaxy flux density longwards of the break feature at 4000Å.

or H α .) Thus the current study comprises three samples at redshifts of $z \sim 0.4$, 1 and 2, using filters which approximate to standard I , J and H -bands respectively. At the time of writing the WFPC2 observations of the sample at $z \sim 0.4$ were incomplete. Hence, the current paper deals only with the NICMOS observations of the two high- z quasar samples.

Since, at each redshift, our chosen filter corresponds to rest-frame V -band, this observing strategy also obviates the need for k -corrections when calculating host-galaxy luminosities. Absolute V -band magnitudes can be calculated directly from the observed R , I , J and H magnitudes without the need to assume any particular spectral shape (and hence stellar population) for the hosts.

2.1.3 Radio loudness

In order to attempt a meaningful comparison of the properties of RLQ and RQQ hosts as a function of redshift we selected five radio-loud and five radio-quiet quasars in each redshift regime, giving a total of 30 objects. In order to perform a clean comparison of the hosts of RLQs and RQQs at each epoch it was important to ensure that the RLQs are genuinely radio-loud ($P_{5GHz} > 10^{25} \text{WHz}^{-1} \text{sr}^{-1}$), that the RQQs are genuinely radio-quiet ($P_{5GHz} < 10^{24.5} \text{WHz}^{-1} \text{sr}^{-1}$), and that within each redshift bin the optical luminosity distributions of the two types are well matched. This is not a trivial task. It requires that we select only RQQs which have been observed with the VLA with high sensitivity but have not been detected, and requires that we confine our RLQ sample to steep-spectrum objects whose intrinsic radio luminosity is not being artificially boosted by relativistic beaming.

The relatively small number of optically-faint steep-spectrum RLQs, along with our stringent definition of radio quietness (few RQQs have been observed with sufficient sensitivity in the radio to meet our self-imposed luminosity requirement), means that the resulting three quasar samples at $z \sim 0.4$, 1 & 2 (illustrated in Figure 1) are almost uniquely defined.

2.2 Observing strategy

2.2.1 Choice of detector

NICMOS contains three HgCdTe arrays, NIC1, NIC2 and NIC3, each consisting of 256×256 pixels. Unlike CCDs, each pixel in the array is independent of its neighbours and can be read non-destructively, allowing multiple read-outs to be performed throughout the duration of a single exposure. This ability can be utilised for the recognition and removal of cosmic ray events during the course of the exposure.

We opted to use NIC1, the smallest of the three detectors, with a field of view $11'' \times 11''$ in extent. The NIC1 PSF is diffraction limited for wavelengths $\geq 1 \mu\text{m}$ and its $0.043''$ pixels guarantee critical sampling of the PSF over the wavelength range of interest.

2.2.2 Integration times

A total of 60 orbits of HST time was allocated for this project. From this total, 11 orbits were devoted to the WFPC2/F814W observations of the 10 quasars in the $z \sim 0.4$ sample as well as a suitable PSF star, leaving 49 orbits for the two high- z NICMOS samples. Simulations using

Table 1. Summary of the quasar samples observed in the current NICMOS study. RQQs are derived from the UVX survey by Boyle et al. (1990) (SGP) and the survey of Marshall et al. (1984) (BVF), and are confirmed as radio quiet ($P_{5GHz} < 10^{24.5} \text{W Hz}^{-1} \text{sr}^{-1}$) by the VLA FIRST & NVSS surveys. RLQs were selected from the Véron-Cetty & Véron (1993) quasar catalogue, with reported 5 GHz radio luminosities $P_{5GHz} > 10^{25} \text{W Hz}^{-1} \text{sr}^{-1}$ and steep radio spectra. V -band magnitudes are from various sources, and where necessary have been converted from B -band measurements. For the estimation of luminosities at both radio and optical wavelengths we have assumed a quasar spectrum of the form $f(\nu) \propto \nu^{-0.5}$

Name	Type	J2000 Position		z	V	Observing date (dd/mm/yy)	Time on source (sec)
		RA ($h m s$)	Dec $^{\circ} ' ''$				
<i>J</i> -band (F110M) sample ($z \sim 1$)							
SGP5:46	RQQ	00 52 22.76	-27 30 02.8	0.955	18.88	25/08/97	1×2048
SGP2:47	RQQ	00 53 02.24	-29 12 55.5	0.830	17.17	14/08/97	1×2048
BVF225	RQQ	13 04 10.47	+35 36 50.8	0.910	18.54	16/02/98	1×2048
BVF247	RQQ	13 05 05.04	+35 51 20.6	0.890	18.73	15/02/98	1×2048
BVF262	RQQ	13 05 30.91	+35 17 13.5	0.970	18.57	18/02/98	1×2048
PKS0440-00	RLQ	04 42 38.64	-00 17 43.4	0.844	18.41	11/08/97	1×2048
PKS0938+18	RLQ	09 41 23.17	+18 21 06.0	0.943	18.49	18/02/98	1×2048
3C422	RLQ	20 47 10.39	-02 36 22.5	0.942	18.69	03/11/97	1×2048
MC2112+172	RLQ	21 14 56.68	+17 29 22.7	0.878	17.89	30/10/97	1×2048
4C02.54	RLQ	22 09 32.82	+02 18 40.9	0.976	18.19	05/11/97	1×2048
SA107-626	PSF star	15 40 05.31	-00 17 29.2	0	12.77	30/07/97	8×256
SA107-627	PSF star	15 40 07.45	-00 17 23.0	0	13.47	17/02/98	8×256
<i>H</i> -band (F165M) sample ($z \sim 2$)							
SGP2:36	RQQ	00 51 14.32	-29 05 19.7	1.756	19.62	20/11/97	3×2048
SGP2:25	RQQ	00 52 07.60	-29 17 50.2	1.868	19.55	28/08/97	4×2048
SGP2:11	RQQ	00 52 38.47	-28 51 12.9	1.976	19.77	02/09/97	4×2048
SGP3:39	RQQ	00 55 43.41	-28 24 09.7	1.964	19.65	06/09/97	4×2048
SGP4:39	RQQ	00 59 08.88	-27 51 24.7	1.716	19.64	30/08/97	3×2048
1148+56W1	RLQ	11 50 44.8	+56 32 56.0	1.782	19.69	30/06/97	4×2048
PKS1524-13	RLQ	15 26 59.44	-13 51 01.3	1.687	19.69	31/07/97	4×2048
B2-2156+29	RLQ	21 58 42.0	+29 59 08.0	1.759	19.29	05/11/97	3×2048
PKS2204-20	RLQ	22 07 33.94	-20 38 34.9	1.923	19.49	04/09/97	4×2048
4C45.51	RLQ	23 54 22.27	+45 53 05.2	1.992	19.79	14/11/97	4×2048
SA107-626	PSF star	15 40 05.31	-00 17 29.2	0	12.77	17/02/98	4×256
SA107-627	PSF star	15 40 07.45	-00 17 23.0	0	13.47	30/07/97	4×256

the 2-D modelling algorithm developed for the analysis of our previous HST study of quasar hosts at $z \sim 0.2$, along with pre-launch predictions of the sensitivity of NICMOS through the F110M and F165M filters indicated that in order to detect host galaxies comparable in size and luminosity to those found at low redshift we would require one orbit per object for the sample at $z \sim 1$ and three to four orbits per object at $z \sim 2$ (the final allocation of orbits is shown in Table 1). Two orbits were reserved for observations of PSF stars through each of the two NICMOS filters (see below).

The NICMOS detectors allow several standard observing modes, taking advantage of the non-destructive read-out capabilities of the detector arrays. We chose to use one of the pre-defined ‘multi-accumulate’ (MULTIACCUM) sequences, with a total of 25 readouts at specific intervals during each integration, which combine high sensitivity with large dynamic range and the ability to process cosmic rays and reconstruct saturated regions of the image. The sequence used was MIF2048 which, with an integration time of 2048 seconds, was the longest sequence which would fit into a single orbit.

2.2.3 Determination of the NICMOS point-spread function

Any attempt to determine the properties of a faint, diffuse object surrounding a much brighter point source ultimately depends on our ability to separate the emission which is genuinely spatially extended from light from the central source which has been artificially spread out by the point-spread function (PSF) of the instrument. Because of the extreme sensitivity of this process to the exact form of the PSF it is vitally important that this is accurately known. This urgency is compounded by the fact that the PSF is a complicated function of the filter used and the SED of the target as well as the position of the object within the aperture.

On-orbit verification and calibration of the NICMOS instrument did not include the acquisition of empirical PSFs for every combination of filter and camera. Synthetic PSFs, although normally an excellent match in the bright central regions, are often less good at reproducing the faint outer wings of the structure and usually fail to account for the effects of instrumental defects and uncertainties. We therefore used two orbits of our allocated HST time to obtain deep NICMOS stellar PSFs in both our chosen filters, F110M and F165M. To safeguard against the possibility of Vega-like circumstellar dust shells which would compromise the PSF, we observed two different stars, SA 107-626 and SA 107-

627. The stars have absolute magnitudes, M_V , of 13.47 and 13.34 respectively, enabling us to obtain high-dynamic range images of each star, tracing the PSF much further into the wings than the quasar exposures, in under half an orbit. Observations with the United Kingdom Infrared Telescope (UKIRT) in April 1997 confirmed that the $J - K$ colours of the stars were 0.60 and 0.48 respectively - and thus a good match to the expected quasar SED within our chosen filter bands.

3 NICMOS DATA REDUCTION

The data were calibrated using the standard NICMOS pipeline software, CALNICA, together with the most recent calibration files. However, certain peculiarities of the NICMOS Camera 1 detector were not adequately compensated for by the pipeline and had to be dealt with separately. The most important of these were the problems of cosmic ray persistence and the residual DC ‘pedestal’.

3.1 Cosmic ray persistence

Since the declinations of our target quasars typically meant that they would be visible for 3300 seconds per orbit the period of visibility remaining after the main MIF2048 exposure and associated read time was utilised for an additional 512-second exposure (using the pre-defined MIF512 sequence). This exposure was placed at the beginning of the orbit and was used to identify any ‘persistent’ cosmic ray tracks which had not been completely flushed from the detector before the start of the observations. Cosmic ray persistence is a particular problem in those observations which take place immediately after one of the spacecraft’s periodic passages through the South Atlantic Anomaly, but can also occur at any point on HST’s orbit. Unlike cosmic rays which impact during a science exposure, the persistent tracks cannot be removed by comparing adjacent readouts of a MULTI-ACCUM sequence because they are present on the detector before the sequence begins. These ghost images generally decay on a timescale of ~ 500 seconds, so by placing a short exposure at the beginning of the orbit we ensured that the problem was largely alleviated by the time the longer science exposure began. Any remaining cosmic rays were then identified by comparison of the MIF512 and MIF2048 exposures since, unlike ordinary cosmic ray tracks, they appear in both images.

3.2 DC offset

Of particular importance to the current study is the effect known as the ‘pedestal’. This is a time- and temperature-dependent DC offset arising from the design of the NICMOS3 array and amplifier system. Its properties are well understood (Rieke et al. 1993), and in principle the effects can be entirely removed as long as contemporaneous dark frames, made at the same detector temperature as the science exposures, are available. Where such contemporaneous darks are not available - as in the present observations - a residual DC offset or ‘pedestal’ remains in the NICMOS images after the subtraction of the dark reference file. This offset propagates throughout the subsequent calibration steps

and leads, ultimately, to a (small) multiple of the flat-field reference file being imprinted onto the final image. Since the flat field contains spatial structure on scales of ~ 1 arcsec, similar to the expected scalelengths of galaxies at redshifts of 1 to 2, removing the effects of the pedestal was a priority.

The severity of the pedestal was reduced by an on-orbit correction applied to all data taken after 12 August 1997, and by the construction of synthetic dark reference files which were often better able to account for the remaining offset. However, the effect is still present to varying degrees in all of the NICMOS images in our study, and these corrections do not apply to the three quasars in our program which were imaged prior to 12 August 1997: SGP2:47 ($z = 0.83$), PKS0440-00 ($z \sim 0.844$) and PKS1524-13 ($z \sim 1.687$). The data quality for these objects is significantly worse than for the rest of the sample.

In order to alleviate this problem, staff at the Space Telescope Science Institute have devised a procedure called *pedtherm* which can be used to estimate and remove the DC offset in each quadrant of an image prior to flat-fielding in CALNICA. Recalibrating our data using this extra step led to significant reduction in the pedestal effect, but failed to remove it entirely.

In a final attempt to reduce the impact of the pedestal still further, each of the calibrated NICMOS images was subjected to an additional corrective procedure devised by ourselves. This algorithm yielded a retrospective estimate of the height of the remaining pedestal by insisting that the standard deviation across object-free regions of the final flat-fielded image was minimized. Most of the images were noticeably improved by this final reduction step, though it proved impossible to remove the pedestal entirely and its effects are particularly evident in images in which the quasar is positioned close to the boundary of two quadrants (BVF225 & SGP2:11).

For the $z \sim 2$ quasar sample three or four separate 2048-second H -band exposures were obtained for each object. Each exposure was calibrated and treated for the pedestal effect separately before being co-added to produce the final image.

3.3 Other problems affecting image quality

Particulate contaminants (believed to be small flecks of paint) on the surface of the NICMOS detector give rise to several regions of reduced sensitivity, each typically a few pixels in extent. The positions of these contaminants are accurately known, allowing the affected pixels to be masked out. A further problem affects the upper left-hand quadrant of the NIC1 array, a significant area of which has a sensitivity 2-3 times lower than the mean of the detector as a whole. The default pointing for NIC1 placed the majority of our target quasars in the lower right-hand quadrant, thus avoiding this problem in most cases. Only the RLQ 4C45.51 from the $z \simeq 2$ sample fell into the affected region and thus suffers from a somewhat higher noise level than the rest of the sample.

Source	z	$r_{1/2}/\text{kpc}$	$\mu_{1/2}$	J_{host}	J_{nuc}	$L_{\text{nuc}}/L_{\text{host}}$	b/a
Radio-Quiet Quasars							
SGP5:46	0.955	3.9	21.65	20.10	19.46	1.79	1.14
SGP2:47	0.830	-	-	-	-	-	-
BVF225	0.910	17.1	23.78	20.11	17.91	7.61	3.20
BVF247	0.890	11.9	22.83	18.88	20.14	0.31	1.20
BVF262	0.970	4.6	21.56	19.85	19.24	1.76	1.36
Radio-Loud Quasars							
PKS0440-00	0.844	13.0	22.71	18.84	18.47	1.41	1.64
PKS0938+18	0.943	4.3	21.10	19.49	19.81	2.29	1.33
3C422	0.942	17.0	22.88	18.29	17.90	1.43	1.33
MC2112+172	0.878	17.4	23.14	18.18	18.97	0.48	1.02
4C02.54	0.976	10.4	21.62	19.32	17.61	4.82	4.08

Table 2. Results from the two-dimensional modelling of the $z \simeq 0.9$ quasar sample. The table gives the fits achieved using an $r^{1/4}$ (de Vaucouleurs) model for the galaxy’s surface brightness profile, and assuming a cosmology with $H_0 = 50 \text{ km s}^{-1}\text{Mpc}$ and $\Omega_m = 1.0$, $\Omega_\Lambda = 0.0$. Column 3 lists the half-light radius, $r_{1/2}$, of the host and column 4 the surface brightness, $\mu_{1/2}$, at this radius (J magnitudes arcsec^{-2}). Columns 5, 6 & 7 list the apparent host and nuclear J -band magnitudes (with associated uncertainties of ~ 0.4 and ~ 0.3 magnitudes respectively) and the ratio of nuclear to host-galaxy luminosity, whilst column 8 gives the axial ratio of the host.

4 DATA ANALYSIS

In this section we describe the process by which information about the underlying host galaxies was extracted from the NICMOS images of the quasars.

4.1 The $z \simeq 1$ sample

In most cases the presence of a significant component of extended emission underlying the nuclear point source can be inferred simply from a visual inspection of the J -band quasar images. The evidence is particularly obvious between radii of 0.1 and 0.2 arcsec from the nucleus, where the first minimum in the NICMOS PSF occurs.

Simple subtraction of a scaled stellar PSF provides further evidence for the presence of an extended component in the majority of the quasar images, and an example of a PSF-subtracted image is shown in Figure 2. However, in order to accurately describe the distribution of this extended light we applied the algorithm developed for the analysis of our previous HST/WFPC2 images of low-redshift quasars (McLure et al. 1999; Dunlop et al. 2001). Full details of this algorithm are given by McLure, Dunlop & Kukula (2000). The algorithm uses χ^2 -minimization to match a synthetic quasar+host to the HST image, with nuclear luminosity, galaxy luminosity, galaxy scalelength, axial ratio, and position angle as free parameters. The galaxy’s surface-brightness profile can be set to either an exponentially decaying (disc) function or an $r^{1/4}$ de Vaucouleurs law (characteristic of an elliptical galaxy) and the resulting fits compared to determine the morphology of the underlying stellar population. In practice, in the majority of the NICMOS images the noise was too high to allow us to distinguish between a disc or an elliptical profile with statistical confidence. In the case of the three most prominent host galaxies (BVF247, BVF262 and PKS0938+18) the preference for a de Vaucouleurs profile was more marked and we show the results of these fits in Figure 3, but the formal significance of this preference is only marginal.

Table 2 lists the results of 2-D modelling for all ten of the F110M (J -band) images, assuming an $r^{1/4}$ de Vau-

couleurs surface-brightness profile. Note that the software could not converge on an acceptable fit for the RQQ SGP2:47, the image with the worst residual pedestal problems. Despite the failure to unambiguously determine the morphologies of the $z \sim 1$ quasar hosts, in most other respects these galaxies do appear to be consistent with the elliptical hosts uncovered for comparably luminous quasars at $z \simeq 0.2$ by our R -band WFPC2 HST study (McLure et al. 1999; Dunlop et al. 2001). Half-light radii range from ~ 4 to 20 kpc and nuclear-to-host luminosity ratios are typically 1 – 2 (the RQQ BVF225 appears to have an unusually high nuclear:host ratio $\simeq 8$ but the image is unusually noisy and the resulting model fit is poorly constrained). We note that the distribution of axial ratios of the hosts peaks at a value of $b/a \sim 1.2$, consistent with them being drawn from a population of elliptical galaxies (Sandage, Freeman & Stokes 1970; Ryden 1992).

4.2 The $z \simeq 2$ sample

Analysis of the H -band (F165M) images of the $z \sim 2$ quasars proved far more problematic. One object, the RLQ 1148+56W1, was not detected due to a combination of positional uncertainty and the HST pointing errors. For the remaining nine quasars, despite the fact that the nominal sky background at H is little different to that at J , by selecting objects of the same absolute magnitudes as those at lower redshifts, the apparent brightness of the targets had of course decreased substantially.

These factors, coupled with the wider H -band PSF, meant that clear evidence for an extended component was immediately apparent in only two of the images (the RQQ SGP2:36 and the RLQ B2-2156+29). In several objects careful subtraction of a scaled PSF does reveal the presence of an underlying extended component although, as the example shown in Figure 4 demonstrates, very little useful information on the quantity and extent of the emission can be derived from this relatively crude procedure.

In order to carry out a more rigorous search for the presence of underlying galaxies we performed 2-D modelling of the H -band images using the algorithm described in the

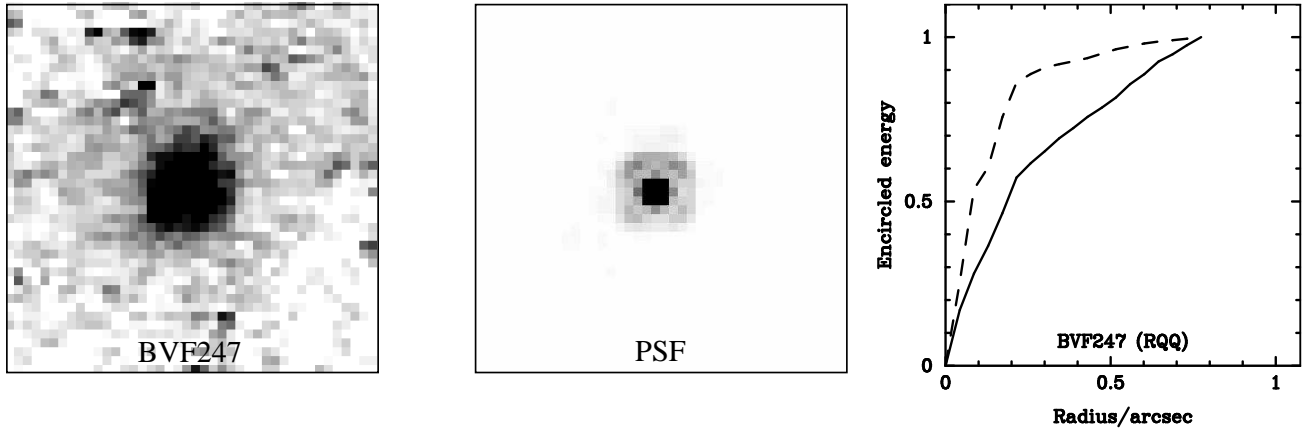


Figure 2. Results of PSF subtraction on the quasar BVF247. The left-hand panel shows the J -band image of the quasar after subtraction of a stellar PSF. Prior to subtraction the PSF was re-centred and scaled such that the value of the central pixel was 0.84 times that of the corresponding pixel in the quasar image. Using a larger PSF:quasar ratio leads to an over-subtracted image in which the flux ceases to rise monotonically towards the centre, causing a characteristic dip in the values of the central few pixels. The image is $1''.75 \times 1''.75$ in size, with greyscale levels extending from 0% (white) to 25% (black) of the maximum flux in the image. The central panel shows the NICMOS J -band PSF, with an identical greyscale cut from 0% to 25% of the peak. The PSF is considerably more compact at the 25% level than the subtracted quasar image, which clearly contains a significant component of extended emission underlying the quasar point source. The right-hand panel shows a normalised encircled energy diagram for the *unsubtracted* quasar image. The plot shows the cumulative flux in a circular aperture of increasing radius (with increments of one pixel), centred on the brightness peak and normalised at the radius at which the background noise in the quasar image becomes significant (defined here to be the radius beyond which the enclosed flux ceases to increase monotonically). The solid line shows the quasar point source plus underlying host galaxy whilst the dashed line shows the equivalent curve for a pure (stellar) PSF. The shallower slope of the quasar profile is further evidence of an underlying extended flux component.

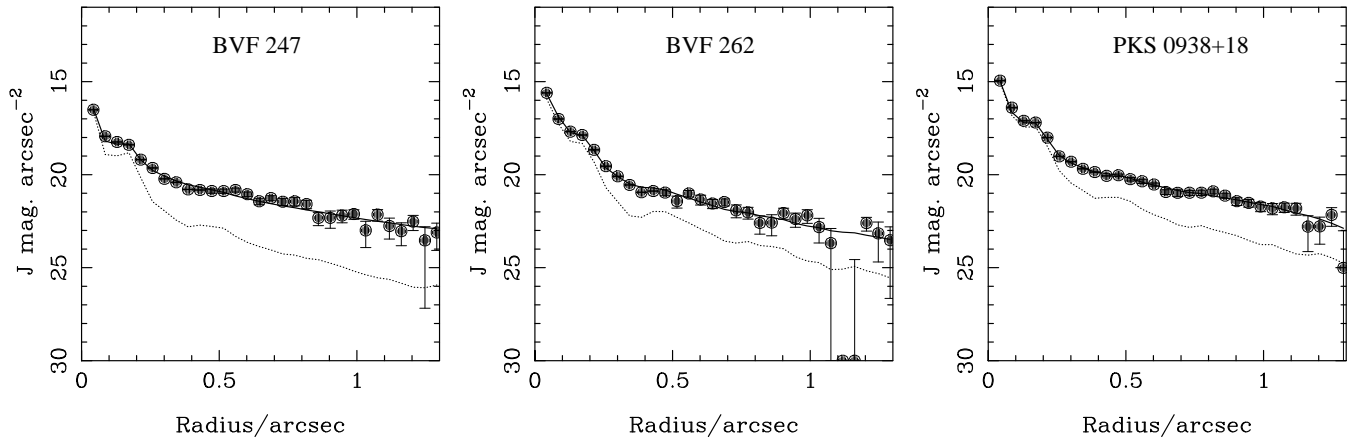


Figure 3. Examples of azimuthally-averaged surface-brightness profiles for three members of the $z \sim 1$ quasar sample observed through the F110M filter (from left to right: the RQQs BVF247 & BVF262 and the RLQ PKS0938+18). In each case the upper (solid) line shows the best-fitting model (galaxy plus quasar), whilst the lower, dotted line shows the contribution due to the nuclear (quasar) component only. In all cases the fit was obtained by assigning a de Vaucouleurs ($r^{1/4}$) law to the host galaxy. Model parameters for each object are listed in Table 2.

previous subsection. As before, we assumed an $r^{1/4}$ (de Vaucouleurs) surface brightness profile for the putative galaxy and used our stellar H -band image to represent the NICMOS PSF. The results of this 2-D modelling are listed in Table 3.

For two objects, the RLQs B2-2156+29 & 4C45.51, the model rapidly converged on a solution, finding luminous, extended galaxies (half-light radii ~ 2 arcsec). For the remaining seven objects, in order to obtain an adequate 2-D fit to the images the algorithm once again found it necessary to include some extended emission in addition to the quasar PSF. However, the algorithm experienced difficulty in converging on a unique solution for the underlying galaxy. The

problem was identified as an inability to determine the luminosity and scalelength of the galaxy simultaneously, due to the fact that the amount of extended flux was generally low, and its distribution lay well within the wings of the H -band point spread function.

In order to encourage the algorithm to converge on a unique solution we reduced the number of free parameters by using a circular galaxy model and fixing the scalelength at either 5 or 10 kpc. By comparing the quality of the resulting fits we could assess whether the ‘small’ or ‘large’ galaxy model gave a better match. In three cases, the RQQ SGP2:36 and the RLQs PKS1524–14 & PKS2204–20, this produced a significant preference for the smaller, 5 kpc model. Note

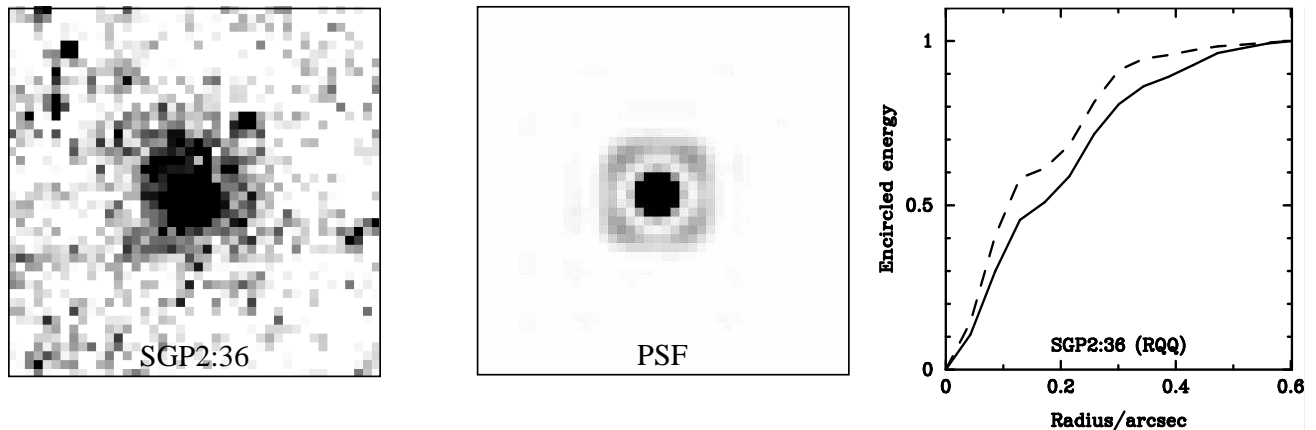


Figure 4. Results of PSF subtraction on the quasar SGP2:36. The left-hand panel shows the H -band image of the quasar after subtraction of a stellar PSF. Prior to subtraction the PSF was re-centred and scaled such that the value of the central pixel was 0.8 times that of the corresponding pixel in the quasar image. Using a larger PSF:quasar ratio results in an over-subtracted image. The image is $1''.1 \times 1''.1$ in size, with greyscale levels extending from 0% (white) to 25% (black) of the maximum flux in the image. The central panel shows the NICMOS H -band PSF, with an identical greyscale cut from 0% to 25% of the peak. Although the difference is less marked than in the J -band example of Figure 2, the residual flux in the subtracted image is more extended than the PSF and cannot be accounted for by a point source. The right-hand panel shows a normalised encircled energy diagram for the *unsubtracted* quasar image. The plot shows the cumulative flux in a circular aperture of increasing radius (with increments of one pixel), centred on the brightness peak and normalised at the radius at which the background noise in the quasar image becomes significant (defined here to be the radius beyond which the enclosed flux ceases to increase monotonically). The solid line shows the quasar point source plus underlying host galaxy whilst the dashed line shows the equivalent curve for a pure (stellar) PSF. The slope of the quasar curve is less steep than that for the pure PSF, providing further evidence for an extended component of emission underlying the quasar point source.

Source	z	$r_{1/2}/\text{kpc}$	H_{host}	H_{nuc}	$L_{\text{nuc}}/L_{\text{host}}$	b/a
Radio-Quiet Quasars						
SGP2:11	1.976	? (<10)	20.65	18.97	4.70	-
SGP2:25	1.868	? (<10)	19.89	19.60	1.31	-
SGP2:36	1.756	~ 5	19.74	19.98	0.80	-
SGP3:39	1.964	? (<10)	19.77	19.55	1.16	-
SGP4:39	1.716	? (<10)	21.60	18.86	12.43	-
Radio-Loud Quasars						
PKS1524–13	1.687	~ 5	19.36	18.10	3.22	-
B2-2156+29	1.753	16.0	17.87	17.97	0.91	1.77
PKS2204–20	1.923	~ 5	20.66	18.57	6.87	-
4C45.51	1.992	17.9	17.86	17.48	1.42	1.23

Table 3. Results from the two-dimensional modelling of the $z \simeq 2$ quasar sample. The table gives the fits achieved using an $r^{1/4}$ (de Vaucouleurs) model for the galaxy’s surface brightness profile, and assuming a cosmology with $H_0 = 50 \text{ km s}^{-1} \text{ Mpc}$ and $\Omega_m = 1.0$, $\Omega_\Lambda = 0.0$. Column 3 lists the half-light radius, $r_{1/2}$, of the host galaxy for those objects in which the model was able to converge on a definite value. For SGP2:36, PKS1524–13 and PKS2204–20 the model showed a preference for a small ($\sim 5 \text{ kpc}$) host, but this value must be treated with caution. For the remaining objects, no reliable estimate of the galaxy size could be obtained, although in view of the low luminosity of the host, they are unlikely to be large. Columns 4, 5, & 6 list the apparent host and nuclear H -band magnitudes (with estimated uncertainties of 0.75 and 0.3 magnitudes respectively) and the ratio of nuclear to host-galaxy luminosity, whilst column 7 gives the axial ratio of the host, where available.

that, though the extended emission in SGP2:36 is clearly visible in the H -band image, the small extent of the galaxy relative to the wings of the H -band PSF was enough to frustrate the modelling software until the number of degrees of freedom was reduced.

For the last four objects neither model gave a significantly better fit to the data, though both gave statistically acceptable results and the flux of the host galaxy remained stable to within ± 0.75 mags. However, in view of the relatively small amount of extended flux, it seems unlikely that the galaxies are much larger than the FWHM of the NIC-

MOS PSF (0.19 arcsec $\sim 2 \text{ kpc}$). In Table 3 we therefore adopt a tentative upper limit of 10 kpc.

5 DISCUSSION

Despite the difficulty in determining morphologies and, at $z \sim 2$, scalelengths for the quasar hosts, the information obtained from the NICMOS images allows us to compare the galaxies with other types of active and inactive galaxies at the same redshifts and to investigate the link between quasar and galaxy evolution. We first discuss the implications of our relatively robust results at $z \simeq 1$, before considering the

implications of our $z \simeq 2$ results in the context of theories of quasar/galaxy evolution.

5.1 Comparison of RLQ and RQQ hosts at $z \simeq 1$

In our study of low-redshift ($z \sim 0.2$) radio-loud and radio-quiet quasars (McLure et al. 1999, Dunlop et al. 2001, Hughes et al. 2000, Nolan et al. 2001), for quasars with $M_V \leq -24$ we found no statistically significant differences between the host galaxies of the two types of quasar. Both RLQs and RQQs seem to lie in large ($r_{1/2} \sim 10$ kpc, luminous ($L > L^*$) elliptical galaxies with colours and ages consistent with those of inactive massive elliptical galaxies at the same redshift.

At $z \sim 1$, although we are unable to determine the morphology of the galaxies with confidence, we find that once again the properties of the radio-loud and radio-quiet hosts are statistically consistent with one another, although there is some evidence of a trend towards a larger luminosity difference than was found at $z \simeq 0.2$. The mean J -band magnitude for the RLQ hosts is 18.8 ± 0.3 and that of the RQQs is 19.7 ± 0.3 , whilst the mean scalelengths are 12.4 ± 2.4 kpc and 9.4 ± 3.2 kpc respectively. A similar tendency towards somewhat less massive hosts for RQQs was also seen in the $z \simeq 0.2$ sample (McLure et al. 1999; Dunlop et al. 2001), although once again the difference was not statistically significant. McLure et al. speculate that this might indicate that the low- z RQQs contain smaller black holes than their radio-loud counterparts, but are accreting gas with greater efficiency, to produce comparable luminosities. Larger samples will be required at both redshifts in order to determine whether this apparently small but persistent difference is in fact real.

5.2 Comparison of quasar hosts and radio galaxies at $z \simeq 1$

In our previous HST study of quasar hosts at $z \sim 0.2$, as well as radio-loud and radio-quiet quasars we also included a sample of FR II radio galaxies which was carefully matched to the RLQ sample in terms of extended 5 GHz luminosity and radio spectral index (Taylor et al. 1996). This enabled us to compare the properties of the three main types of powerful active galaxy in the local universe, and to test models which claim to unify RLQs and radio galaxies via viewing angle effects. We found that the radio galaxies were indistinguishable from the hosts of RLQs and luminous RQQs, having similar sizes, colours and luminosities and following a Kormendy relation identical to that of normal, inactive massive elliptical galaxies (McLure et al. 1999; Dunlop et al. 2001).

Due to scheduling pressures it was not practical to include a comparison sample of radio galaxies in the current NICMOS study. However, by utilising the data in the HST archive we are able to construct a *post hoc* sample of radio galaxies which is roughly matched to the quasars at $z \sim 0.9$.

Of all the radio galaxy images in the archive the most useful in terms of redshift, radio luminosity and observing waveband are the I -band images of 3CR radio galaxies made with WFPC2 by Best, Longair & Röttgering (1997; 1998). These images have been reanalysed by McLure & Dunlop

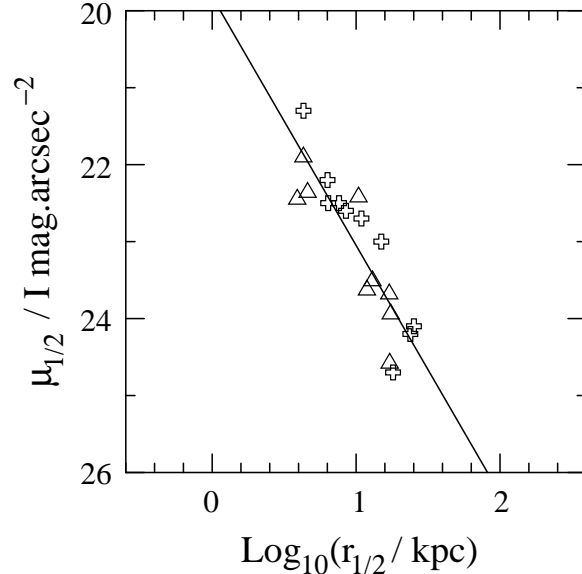


Figure 5. The apparent I -band Kormendy relation described by the $z \sim 1$ quasars (triangles) imaged with NICMOS through the F110M ($\simeq J$) filter. Conversion to I magnitudes has been carried out assuming $I - J$ colours of 0.8, a typical value for elliptical galaxies at $z \sim 1$ (Fasano et al. 1998). Also shown are the $z \sim 0.8$ 3CR radio galaxies from the sample of Best, Longair & Röttgering (1997; 1998) (crosses). These objects were imaged in I -band with WFPC2 on HST and the images reanalysed by McLure & Dunlop (2000) with the same algorithm used to model the NICMOS images in the current study. The solid line shows a least squares fit to the combined samples, and has a slope of 3.23 ± 0.42 (cf 3.5 for the radio galaxies alone).

(2000) with the same 2-D modelling software used to analyse the current NICMOS images. By assuming an $I - J$ colour of 0.8 for elliptical galaxies at $z \sim 1$ (Fasano et al. 1998) it becomes possible to make a comparison between the quasar hosts imaged in J -band with NICMOS and the I -band radio galaxy images.

We find that the I -band properties of the quasar hosts are very similar to those of the radio galaxies: mean scalelengths (with standard errors) are 12.6 ± 2.3 (RGs) and 11.0 ± 1.8 (quasar hosts), whilst the mean absolute I magnitudes are -24.62 ± 0.13 (RGs) and -24.59 ± 0.21 (quasar hosts).

Given that the redshift distributions of the 10-object 3CR galaxy subsample and the new $z \sim 1$ quasar sample are similar, it is also possible to investigate whether their Kormendy relations are compatible, without the need to make surface-brightness corrections. Once again, we can convert the NICMOS J magnitudes for the quasars to I -band values by assuming an $I - J$ colour of 0.8. The two sets of data are shown in Figure 5, where it can be seen that the Kormendy relations for both quasars and radio galaxies are statistically indistinguishable. A least-squares fit to all the data points produces the relationship $\mu_{1/2} = 3.23 \pm 0.42 \log r_{1/2} + 19.82 \pm 0.4$ (for the radio galaxies alone the fit has a slope of 3.5; McLure & Dunlop 2000). Thus at these redshifts both the quasar hosts and radio galaxies appear to be derived from the same parent population. This result is consistent with the unification of RLQs and radio galaxies via viewing-angle effects, a scenario which is already well supported at low redshifts.

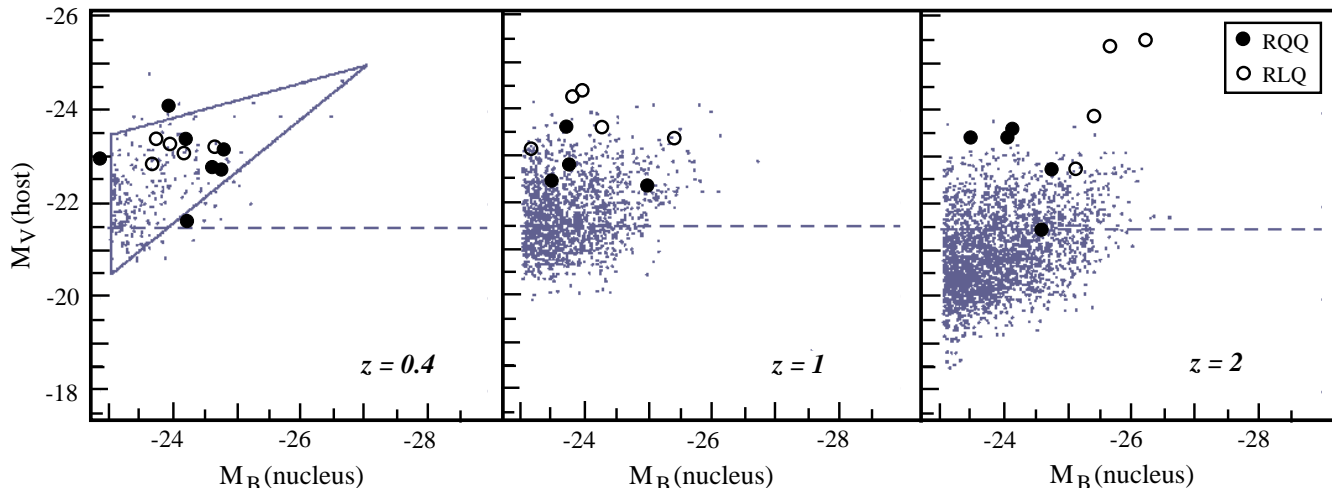


Figure 6. Host galaxy versus quasar (nuclear) absolute magnitudes at redshifts of 0.4, 1 and 2. The dashed line shows the value of L_V^\dagger for galaxies in the local universe. The small grey points are the simulated data from the semi-analytic model of Kauffmann & Haehnelt (2000), showing the predicted evolution of the relationship between M_V of the host and M_B of the active nucleus, and assuming the same cosmology used in the current paper. The large symbols show the results of the current NICMOS study, with filled circles representing RQQs and open circles RLQs. Since we currently lack data for objects at $z = 0.4$, in the left hand panel we plot the subset of RLQs and RQQs with $-24 \geq M_V(\text{total}) \geq -25$ from our WFPC2 study of quasars at $z \sim 0.2$ (McLure et al. 1999; Dunlop et al. 2001). The triangle in the left hand panel shows the locus of the quasar sample of McLeod, Rieke & Storrie-Lombardi (1999). Since at each redshift our chosen filter corresponds to rest-frame V -band, the absolute V -band magnitudes can be calculated directly from the observed R , J and H magnitudes without the need to assume any particular spectral shape for the hosts. For the quasars we have converted from M_V to M_B using a colour index of $B - V = 0.4$ (equivalent to a spectrum of the form $f(\nu) \propto \nu^{-0.2}$). (Figure adapted from Figure 12 of Kauffmann & Haehnelt (2000).)

The lack of bright nuclear point sources in the radio galaxies means that their morphologies can be determined unambiguously; as expected all have radial surface brightness profiles which are well described by a de Vaucouleurs law. Thus, although our analysis of the quasar hosts cannot distinguish between an elliptical or a disc profile with any degree of confidence, their similarity in all other respects to the 3CR radio galaxies provides strong circumstantial evidence that, as at low redshifts, these quasars inhabit massive elliptical galaxies. If this is the case it implies that, just as at low redshift, an important prerequisite for the presence of a powerful AGN at $z \sim 1$ is a host galaxy with a massive spheroidal component. Within the context of hierarchical clustering models for galaxy formation, the similarity (but for passive stellar evolution) between both radio galaxies and quasar hosts at $z \simeq 1$ and their counterparts at $z \simeq 0.2$ is most simply explained by a cosmological model in which the massive elliptical galaxy formation process is essentially complete by $z \simeq 1$.

5.3 The nature of quasar hosts at $z \simeq 2$

The strong cosmological evolution in comoving space density of quasars has been known for nearly 40 years. Much work has gone into empirical fits of the evolution (Schmidt & Green 1983; Boyle, Shanks & Peterson 1988; Dunlop & Peacock 1990; Hewett, Foltz & Chaffee 1993; Goldschmidt & Miller 1998; Goldschmidt et al. 1999) but this has not led to any physical understanding of its causes. Some recent theoretical work (Efstathiou & Rees 1988; Carlberg 1990; Haehnelt & Rees 1993; Percival & Miller 1999) has concen-

trated on explaining the evolution as being driven by evolution in the rate of galaxy merging, following the hypothesis that quasars display a cosmologically short-lived burst, or bursts, of activity following such a merger. Kauffmann & Haehnelt (2000) have used a semi-analytic model to link the growth of supermassive black holes with the formation and evolution of galaxy dark matter halos in a cold dark matter (CDM) universe. They find that the evolution in merger rate of dark halos alone cannot explain the large evolution in quasar space density, in agreement with the analytic work of Percival & Miller (1999). They suppose that accretion timescale also varies with cosmic epoch, and thus they effectively add a component of luminosity evolution onto the basic model (as also proposed by Haehnelt & Rees 1993) which can successfully reproduce the approximately luminosity evolution that is observed (Boyle et al. 2000). Within this framework, quasars of a given luminosity are powered by progressively lower-mass black holes with increasing redshift. Hence if black-hole mass is indeed related to the mass of the dark halo, as might be implied from the correlations between black-hole mass and galaxy bulge luminosity (Kormendy & Richstone 1995; Magorrian et al. 1998; van der Marel 1999) and between black-hole mass and galaxy velocity dispersion (Ferrarese & Merritt 2000; Gebhardt et al. 2000), the Kauffmann & Haehnelt (2000) model predicts that quasars of a given luminosity should, on average, be found in progressively less massive host galaxies with increasing redshift. In fact, provided that a relationship between black-hole mass and host galaxy mass exists at all redshifts, then any luminosity-evolution model will predict such an effect, and this prediction can now be tested.

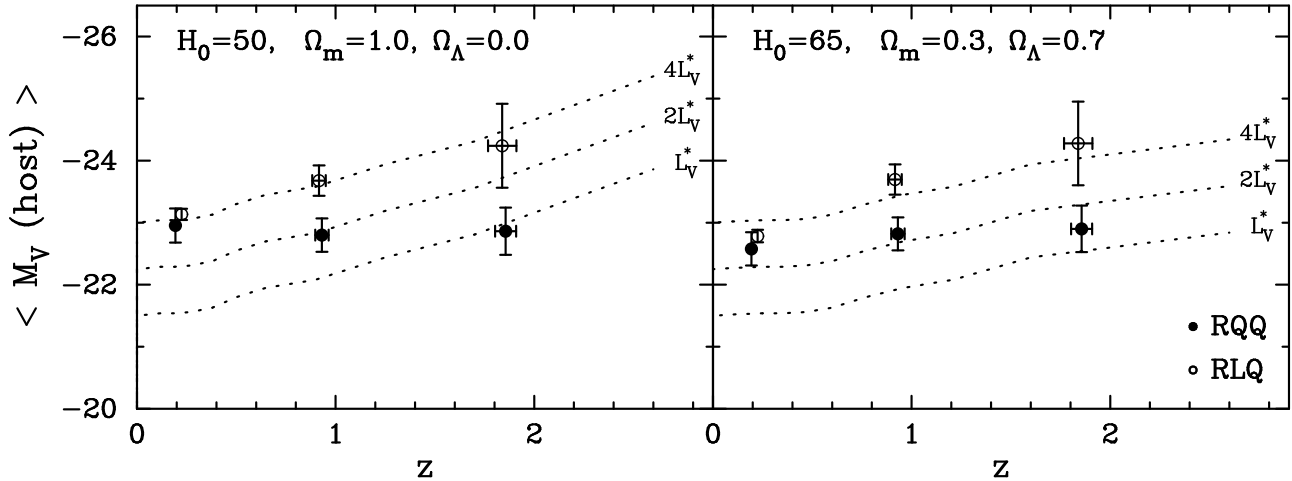


Figure 7. Mean absolute V -band magnitude versus mean redshift for the host galaxies of the RLQs (open circles) and RQQs (filled circles) in the current NICMOS study. Also shown is the subset of 5 RLQs and 7 RQQs from our WFPC2 study of quasars at $z \sim 0.2$ which have total (host + nuclear) luminosities in the same range as the high-redshift samples ($-24 \geq M_V \geq -25$). Error bars show the standard error on the mean. The dotted lines show the luminosity evolution of present day L^* , $2L^*$ and $4L^*$ elliptical galaxies, assuming a formation epoch of $z = 5$ with a single rapid burst of starformation followed by passive evolution thereafter. Left-hand panel: assuming a cosmology with $H_0 = 50 \text{ km s}^{-1} \text{ Mpc}^{-1}$, $\Omega_m = 1.0$ and $\Omega_\Lambda = 0.0$. Right-hand panel: $H_0 = 65 \text{ km s}^{-1} \text{ Mpc}^{-1}$, $\Omega_m = 0.3$ and $\Omega_\Lambda = 0.7$.

To date, ground-based studies have not strongly supported such a picture, finding evidence for very luminous hosts around quasars at redshifts of ~ 2.5 . However, these observations have concentrated on the most luminous quasars, for which there are no counterparts at low redshifts. Our current HST study thus offers the prospect of the first, proper, unbiased view of how host-galaxy luminosity varies with redshift, in a manner which offers a direct and transparent test of theoretical predictions. This is not only because we have studied quasars of similar luminosity at $z \simeq 0.2, 1$ & 2 , but also because we have observed all the hosts at the same rest wavelength (removing the need for k -corrections), and because host-galaxy luminosities have been derived using an identical modelling technique at all redshifts.

In Figure 6 we show the best-fit host and nuclear luminosities for our quasar samples at $z \simeq 0.2, 1$ & 2 superimposed onto the scatterplot predictions for quasars/hosts at $z \simeq 0.4, 1$ & 2 produced by Kauffmann & Haehnelt (2000). As can be seen, the agreement between observation and prediction is excellent for the low-redshift sample, but becomes progressively less convincing within the higher redshift bins as the model predictions recede, while our derived host luminosities remain either roughly constant (in the case of the RQQs) or actually increase with redshift (in the case of the RLQs). We note that the behaviour of the RLQ hosts cannot be explained away simply as the effect of the two unusually luminous RLQs in the $z \simeq 2$ sample. (The V magnitudes quoted in the Véron-Cetty & Véron catalogue are often merely extrapolations based on data in other wavebands, so it is perhaps unsurprising that our sample should turn out to contain two objects slightly more luminous than our nominal upper limit of $M_V(\text{total}) = -25$.) Even when these two objects are excluded, the remaining RLQ hosts at $z \simeq 2$ show no evidence for a drop in luminosity with redshift, and a tendency towards increasing luminosity is clearly already present at $z \simeq 1$.

To clarify the trend of host luminosity with redshift seen

in our sample, we plot mean M_V versus redshift in Figure 7, for two alternative cosmologies, overlaid with the predictions for a passively evolving galaxy formed in a short-lived burst at high-redshift ($z = 5$). Passive evolution commencing at high redshift appears to be the most reasonable starformation history to adopt, given the evidence from Nolan et al. (2001) & de Vries et al. (2000) that low- z quasar hosts and radio galaxies are dominated by stellar populations of age $\simeq 12 \text{ Gyr}$.

These plots demonstrate a number of potentially important points. First, it is clear that in either cosmology the hosts of RLQs brighten with redshift in a manner which is perfectly consistent with pure passive evolution. Basically, the typical host of an RLQ appears to be a passively evolving (present-day) $4L^*$ elliptical. This result agrees well with what has been found for high-redshift radio galaxies. Specifically, if we compare our $z \simeq 2$ results directly with H -band observations of radio galaxies at comparable redshift, the average H -band magnitude for radio galaxies in the redshift band $1.7 - 2.1$ discussed by Lacy, Bunker & Ridgway (2000) is 19.2 ± 0.3 , while the average H -band magnitude for the RLQ hosts in our $z \simeq 1.9$ sample is 18.9 ± 0.7 . Our results for RLQ hosts are also consistent with the findings of a recent ground-based imaging study of three RLQs at $z \sim 1.5$ by Falomo et al. (2001). Taken together, these results therefore provide further support for a picture in which the formation of ellipticals with sufficiently massive black holes to support radio activity (see McLure et al. 1999), is essentially complete before $z \simeq 2$.

The trend displayed by the hosts of RQQs does appear to be somewhat different however. While the error bars have also grown, it seems that the gap between the luminosities of the hosts of RQQs and RLQs has grown still further to $\simeq 1.5$ magnitudes, simply because the typical RQQ host in our sample appears to have the same absolute magnitude at all redshifts.

The interpretation of this observation is dependent on

choice of cosmology. In the flat matter-dominated cosmology, the RQQ hosts are inconsistent with having had a constant mass in stars which has evolved passively since $z = 5$. Evaluation of any change in mass then depends on the choice of star-formation history, but is a factor of 4 under the assumption of passive stellar evolution between $z \simeq 2$ and the present day. In the Λ -dominated cosmology, the RQQ hosts are in fact consistent with no change in mass. Thus, even accounting for the apparent difference between RLQ and RQQ hosts at $z \sim 2$, the large variation in typical host mass with redshift predicted by Kauffmann & Haehnelt (2000) is not observed.

Recent results from other studies of the hosts of high-redshift RQQs also indicate that they are less luminous than their radio-loud counterparts. In particular, Ridgway et al. (2001) report results from NICMOS imaging of 5 RQQs at $z \simeq 2 - 3$, in which they find host galaxies with typical luminosities of $\sim L^*$. In fact two of their RQQs are rather fainter than those discussed here, and if one confines attention to the three objects in their sample with $M_B \simeq -24$ their PSF-subtracted host luminosities are $\simeq 2L^*$. Any subsequent correction for PSF over-subtraction would only raise these values further, guaranteeing rather good agreement with the results shown in Figure 7.

Other preliminary NICMOS-based results on the luminosities of RQQ hosts at $z \simeq 2$ have been presented by Rix et al. (1999), as an interesting by-product of the CfA-Arizona-Gravitational-Lens-Survey (CASTLES). This study attempts to measure the host luminosities of RQQ in strongly lensed systems, by correcting the observed extended emission for the effects of the gravitational lensing, and it has been claimed that their results mirror exactly the predictions of Kauffmann & Haehnelt (2000). Such a conclusion may be premature since it is hard to assess the surface brightness biases inherent in this method, but nonetheless it seems unlikely that the derived RQQ host luminosities could be sufficiently underestimated (by ~ 2 mags) to be consistent with the hosts of RLQs and radio galaxies.

It thus seems hard to avoid the conclusion that there exists a real difference of $\simeq 1$ mag. between the hosts of radio-loud and radio-quiet AGN of comparable nuclear optical luminosity at $z \simeq 2$.

5.4 Implications

These results raise two fundamental questions. First, what are the implications of the observed rather modest drop in RQQ host mass as a function of redshift? Second, why is a comparable drop in host mass not apparent for the RLQs?

The answer to the first question is that, provided the relationship between black-hole and host-spheroid mass is basically unchanged out to $z \simeq 2$, our results exclude any model of quasar evolution which involves a substantial component of luminosity evolution. This is because the rather modest drop in RQQ host mass with increasing redshift implies that a typical RQQ black-hole power source at $z \simeq 2$ is only radiating $\simeq 2 - 3$ times more efficiently than at low-redshift. This is obviously completely at odds with pure luminosity evolution models which, to explain the evolution of the quasar optical luminosity function, require black holes to radiate $\simeq 30$ times more efficiently at $z \simeq 2$. However, it is also in conflict with more topical and apparently more

realistic models, such as the hierarchical models of Kauffmann & Haehnelt (2000), which still require a substantial (order-of-magnitude) component of luminosity evolution to be invoked to explain the rapid evolution of the quasar luminosity function (e.g. Boyle et al. 2000).

Our results are much more consistent with a picture in which the increased availability of fuel (or, equivalently, increased frequency of mergers) at $z \simeq 2$ results in a substantial increase in the number density of active black holes, along with a moderate increase in the fueling efficiency of a typical observed quasar. An increase of a factor of 2-3 in typical fueling efficiency between $z \simeq 0.2$ and $z \simeq 2$ is certainly permitted by the results of detailed studies of black-hole masses in nearby RQQs (Dunlop et al. 2001; McLure et al. 2001), which suggest that on average RQQs at $z \simeq 0.2$ are radiating at only $\simeq 20\%$ of their Eddington limit. It is thus not unreasonable to find that, in an era of greater fuel availability, our sample of $z \simeq 2$ RQQs, matched in nuclear optical output to our low-redshift sample, could be largely produced by black-holes (and hence hosted by spheroids) with a characteristic mass a few times smaller than in the comparison $z \simeq 0.2$ sample. Importantly, however, an observed trend towards moderately higher fueling efficiencies with increasing z does not require one to invoke some redshift-dependent change in quasar black-hole accretion mechanism. On the contrary, the observed modest mass reduction is in fact predicted by new models which attempt to explain observed quasar evolution as a consequence of varying quasar birthrate, combined with declining light-curves for individual quasars (Miller, Percival & Lambert, in preparation). In these models, the increased birth-rate at $z \simeq 2$ leads to a statistical bias such that quasars of a given absolute magnitude are more likely to be observed earlier in (i.e. closer to the peak of) their declining light-curves, and therefore closer to maximum luminosity than at low redshift, when quasar birth is relatively rare.

In answer to the second question, one possible explanation is the effect of the joint selection criteria of high radio luminosity and moderate optical luminosity used in the definition of our RLQ sub-samples. There is now growing evidence that luminous radio sources are only produced by a very massive subset of the black-hole population which powers quasars in general. In particular, the results of Dunlop et al. (2001) and McLure & Dunlop (2001) indicate that the RLQs in our $z \simeq 0.2$ sample are powered by black-holes which are typically 3 times more massive than the power sources of RQQs, and are confined to the mass range $M > 10^9 M_\odot$. If this remains true at high redshift, and if the black-hole spheroid relationship remains basically unchanged, then radio-based selection will effectively guarantee host galaxies of similar mass at all redshifts. If, as we have done in this study, one also insists that the optical luminosities of the RLQs under study are comparable at $z \simeq 2$ and $z \simeq 0.2$, then it would not be unexpected that such subsamples of objects would show no evidence for the redshift-dependent change in fueling efficiency found for the RQQs. This does not of course mean that RLQs would not, on average, be more efficiently fueled at high redshift, but rather that the selection criteria used here would mitigate against us observing such an effect in our sample.

6 SUMMARY

We have presented the results of the first, major observational study designed to determine the properties of the hosts of both radio-loud and radio-quiet quasars from $z \simeq 2$ to the present day in a genuinely unbiased manner. The key features of this study are: (i) sufficient HST-based angular resolution to allow a meaningful attempt at determining galaxy scalelengths at all redshifts; (ii) the use of quasar samples with the same characteristic absolute magnitude at all redshifts; (iii) our insistence that the radio-quiet quasars selected for study are known to lie below a definite radio-luminosity threshold; (iv) filter selection, which when coupled with careful sample redshift constraints, guarantees line-free imaging at the same rest-wavelength ($\simeq 5800\text{\AA}$) (removing concerns about emission-line contamination, and obviating the need for k-corrections); (v) the extraction of host-galaxy parameters using an identical modelling approach at all redshifts, minimising potential surface-brightness bias and concerns over aperture corrections; (vi) the use of properly-sampled, high-dynamic-range PSFs derived from observations of stars through the same filters, and on the same regions of the relevant detectors, as the quasar images.

At $z \simeq 1$ we have been able to determine host-galaxy parameters with sufficient accuracy to demonstrate that the hosts of both RQQs and RLQs lie on the same Kormendy relation as deduced for 3CR radio galaxies at comparable redshift by McLure & Dunlop (2000). The hosts of both RLQs and RQQs seem to have changed little, if at all, in terms of size between $z \simeq 1$ and $z \simeq 0.2$. The typical luminosity of the RLQ hosts has increased between $z \simeq 0.2$ and $z \simeq 1$ by an amount that is perfectly consistent with pure passive evolution of a mature stellar population. The typical luminosity of the RQQ hosts is less enhanced, and indeed appears basically unchanged. There is thus a suspicion that the host masses of RQQs of comparable nuclear output are less massive at $z \simeq 1$, but the significance of this result is marginal. Within a Λ -dominated cosmology our results are certainly consistent with the host masses of both class of quasar being unchanged between $z \simeq 1$ and $z \simeq 0.2$.

At $z \simeq 2$, although the hosts are harder to detect and consequently to model, we have found that host-galaxy magnitudes can be extracted with sufficient confidence to demonstrate that the hosts of RLQs continue to brighten as expected under the hypothesis of pure passive evolution of hosts with non-evolving mass. In contrast, the hosts of RQQs again seem little changed in luminosity, and systematically smaller in size compared to at $z \simeq 1$. This apparently growing radio-loud/radio-quiet host-mass gap is mirrored in other studies of radio galaxies and radio-quiet quasars at comparable redshift, lending further support to its reality. Even after allowance for passive evolution, the inferred drop in RQQ host mass is relatively modest compared to the predictions of an order of magnitude drop in mass made by Kauffmann & Haehnelt (2000). The mass drop is a factor of 4 in an Einstein-de-Sitter cosmology, assuming a passive evolution model, and a factor of 2 if $\Omega_m = 0.3$ and $\Omega_v = 0.7$.

The lack of strong evolution in host mass with redshift argues against models of quasar evolution, such as the latter, which invoke some relationship between host mass and quasar luminosity together with substantial luminosity evo-

lution of the quasar component. Rather, this study indicates that the increased availability of fuel at $z \simeq 2$ results in a substantial increase in the number density of active black holes, along with a moderate increase in the fueling efficiency of a typical observed quasar. This type of moderate efficiency increase is certainly permitted by studies of the fueling efficiency of low-redshift quasars (Dunlop et al. 2001; McLure & Dunlop 2001), and indeed arises naturally as a statistical effect predicted by new models which attempt to explain observed quasar evolution as a consequence of varying quasar birthrate, combined with declining light-curves for individual quasars (Miller, Percival & Lambert, in preparation).

ACKNOWLEDGMENTS

The authors would like to thank the referee, D. Hines, for many useful comments and suggestions, and E. Bergeron for help with *pedtherm*. MJK, RJM & WJP acknowledge PPARC funding. JSD acknowledges the enhanced research time afforded by the award of a PPARC Senior Fellowship. Support for this work was provided by NASA through grant numbers GO-06776.01-95A & GO-07447.01-96A from the Space Telescope Science Institute, which is operated by the Association of Universities for Research in Astronomy, Inc., under NASA contract NAS5-26555. Based on observations with the NASA/ESA *Hubble Space Telescope*, obtained at the Space Telescope Science Institute. This research has made use of the NASA/IPAC Extragalactic Database (NED) which is operated by the Jet Propulsion Laboratory, California Institute of Technology, under contract with NASA.

REFERENCES

- Aretxaga I., Boyle B. J., Terlevich R. J., 1995, MNRAS, 275, L27
- Aretxaga I., Terlevich R. J., Boyle B. J., 1998, MNRAS, 296, 643
- Bahcall J. N., Kirhakos S., Schneider D. P., 1994, ApJ, 435, L11
- Bahcall J. N., Kirhakos S., Schneider D. P., 1995a, ApJ, 447, L1
- Bahcall J. N., Kirhakos S., Schneider D. P., 1995b, ApJ, 450, 486
- Bahcall J. N., Kirhakos S., Schneider D. P., 1996, ApJ, 457, 557
- Bahcall J. N., Kirhakos S., Saxe D. H., Scheider D. P., 1997, ApJ 479, 642
- Best P. N., Longair M. S., Röttgering H. J. A., 1997, MNRAS, 292, 758
- Best P. N., Longair M. S., Röttgering H. J. A., 1998, MNRAS, 295, 549
- Boyce P. J., et al., 1998, MNRAS, 298, 121
- Boyle B. J., Shanks T., Peterson B. A., 1988, MNRAS, 235, 935
- Boyle B. J., Fong R., Shanks T., Peterson B. A., 1990, MNRAS, 243, 1
- Boyle B. J., Shanks T., Croom S. M., Smith R. J., Miller L., Loaring N., Heymans C., 2000, MNRAS, 317, 1014
- Carballo R., Sánchez S. F., González-Serrano J. I., Benn C. R., Vigotti M., 1998, AJ, 115, 1234
- Carlberg R., 1990, ApJ, 350, 505
- de Vries W. H., O’Dea C. P., Barthel P. D., Fanti C., Fanti R., Lehnert M. D., 2000, AJ, 120, 2300
- Disney M. J., et al. 1995, Nature, 376, 150
- Dunlop J. S., Taylor G. L., Hughes D. H., Robson E. I., 1993, MNRAS, 264, 455
- Dunlop J. S., McLure R. J., Kukula M. J., Baum S. A., O’Dea C. P., Hughes D. H., 2001, MNRAS submitted

- Dunlop J. S., Peacock J. A., 1990, MNRAS, 247, 19
- Efstathiou G., Rees M. J., 1988, MNRAS, 230, 5P
- Falomo R., Kotilainen J., Treves A., 2001, ApJ, 547, 124
- Fasano G., Cristiani S., Arnouts S., Filippi M., 1998, AJ, 115, 1400
- Ferrarese L., Merritt D., 2000, ApJ, 539, L9
- Gebhardt K., Bender R., Bower G., Dressler A., Faber S. M., Filippenko A. V., Green R., Grillmair C., Ho L. C., Kormendy J., Lauer T. R., Magorrian J., Pinkney J., Richstone D., Tremaine S., 2000, ApJ, 539, L13
- Goldschmidt P., Miller L., 1998, MNRAS, 293, 107
- Goldschmidt P., Kukula M. J., Miller L., Dunlop J. S., 1999, ApJ, 511, 612
- Hamilton T. S., Casertano S., Turnshek D. A., 2001, (astro-ph/0011255)
- Heckman T. M., Lehnert M. D., van Breugel W., Miley G. K., 1991, ApJ, 370, 78
- Hewett P. C., Foltz C. B., Chaffee F. H., 1993, ApJ, 406, 43
- Hintzen P., Romanishin W., Valdes F., 1991, ApJ, 366, 7
- Hooper E. J., Impey C. D., Foltz C. B., 1997, ApJ, 480, L95
- Hughes D. H. et al., 1998, Nature, 394, 241
- Hughes D. H., Kukula M. J., Dunlop J. S., Boroson T., 2000, MNRAS, 316, 204
- Hutchings J. B., 1995, AJ, 110, 994
- Hutchings J. B., Morris S. C., 1995, AJ, 109, 1541
- Kauffmann G., Haehnelt M., 2000, MNRAS, 311, 576
- Kormendy J., Richstone D., 1995, ARA&A, 33, 581
- Lacy M., Bunker A. J., Ridgway S. E., 2000, AJ, 120, 68
- Laor A., 2000, ApJ, 543, L111
- Lehnert M. D., Heckman T., Chambers K. C., Miley G. K., 1992, ApJ, 393, 68
- Lowenthal J. D., Heckman T. M., Lehnert M. D., Elias J. H., 1995, ApJ, 439, 588
- Madau P., Fergusson H. C., Dickinson M., Giavalisco M., Steidel C. C., Fruchter A. S., 1996, MNRAS, 283, 1388
- Magorrian J., et al., 1998, AJ, 115, 2285
- Márquez I., Petitjean P., Théodore B., Bremer M., Monnet G., Beuzit J. -L., 2001, A&A submitted, astro-ph/0103232
- Marshall H. L., Huchra J. P., Tananbaum H., Avni Y., Braccetti A., Zitelli V., Zamorani G., 1984, ApJ, 283, 50
- McLeod K. K., Rieke G. H., 1994a, ApJ, 431, 137
- McLeod K. K., Rieke G. H., 1994b, ApJ, 420, 58
- McLeod K. K., Rieke G. H., 1995, ApJ, 441, 96
- McLeod K. K., Rieke G. H., Storrie-Lombardi L. J., 1999, ApJ, 511, L67
- McLure R. J., Kukula M. J., Dunlop J. S., Baum S. A., O'Dea C. P., Hughes D. H., 1999, MNRAS, 308, 377
- McLure R. J., Dunlop J. S., 2000, MNRAS, 317, 249
- McLure R. J., Dunlop J. S., 2001, MNRAS, in press (astro-ph/0009406)
- McLure R. J., Dunlop J. S., Kukula M. J., 2000, MNRAS, 318, 693
- Nolan L. A., Dunlop J. S., Kukula M. J., Hughes D. H., Boroson T., Jimenez R., 2001, MNRAS, 323, 308
- Percival W. J., Miller L., 1999, MNRAS, 309, 823
- Percival W. J., Miller L., McLure R. J., Dunlop J. S., 2001, MNRAS, 322, 843
- Ridgway S. E., Heckman T. M., Calzetti D., Lehnert M., 2001, ApJ, 550, 122
- Rieke M. J., Winters G. S., Cadien J., Rasche R., 1993, Proc. SPIE, 1946, 214
- Rix H. -W., Falco E., Impey C., Kochanek C., Lehar J., McLeod B., Muñoz J., Peng C., 1999 (astro-ph/9910190)
- Rönnback J., van Groningen E., Wanders I., Örndahl E., 1996, MNRAS, 283, 282
- Ryden S., 1992, ApJ, 396, 445
- Sandage A. R., Freeman K. C., Stokes N. R., 1970, ApJ, 268, 831
- Schade D., Boyle B. J., Letawsky M., 2000, MNRAS, 315, 498
- Schmidt M., Green R. F., 1983, ApJ, 269, 352
- Steidel C. C., Adelberger K. L., Giavalisco M., Dickinson M., Pettini M., 1999, ApJ, 519, 1
- Stockton A., MacKenty J. W., 1987, ApJ, 316, 584
- Tadhunter C. N., Scarrott S. M., Draper P., Rolph C., 1992, MNRAS, 256, 53P
- Taylor G. L., Dunlop J. S., Hughes D. H., Robson E. I., 1996, MNRAS, 283, 930
- van der Marel R. P., 1999, AJ, 117, 744
- Véron-Cetty M. -P., Woltjer L., 1990, A&A, 236, 69
- Véron-Cetty M. -P., Véron P., 1993, ESO Sci. Rep. No. 13
- Warren S. J., Hewett P. C., Osmer P. S., 1994, ApJ, 421, 412

This paper has been produced using the Royal Astronomical Society/Blackwell Science L^AT_EX style file.